



# New MR perfusion features in primary central nervous system lymphomas: pattern and prognostic impact

Stella Blasel<sup>1</sup> · Rieke Vorwerk<sup>1</sup> · Makoto Kiyose<sup>1,3</sup> · Michel Mittelbronn<sup>5,8,9,10,11</sup> · Uta Brunnberg<sup>12</sup> · Hanns Ackermann<sup>13</sup> · Martin Voss<sup>4</sup> · Patrick N. Harter<sup>5,6,7</sup> · Elke Hattingen<sup>1,2</sup>

Received: 9 November 2017 / Revised: 30 December 2017 / Accepted: 4 January 2018 / Published online: 30 January 2018  
© Springer-Verlag GmbH Germany, part of Springer Nature 2018

## Abstract

**Purpose** Some MR perfusion features predict overall survival (OS) and progression-free survival (PFS) in glioblastomas. Prognostic value of MR perfusion in primary CNS lymphomas (PCNSL) remains unexplored being the aim of this investigation.

**Methods** We retrospectively analyzed 3Tesla dynamic susceptibility contrast MR perfusion in 37 pre-surgical PCNSL for normalized regional cerebral blood volume  $rCBV_{mean}$  and  $rCBV_{max}$  and for a PCNSL-typical shoulder-like increase of the time–signal intensity curve (“TSIC-shoulder”), indicating moderate vessel permeability. These MR perfusion features, tumor and edema size, number of lesions and patient characteristics were correlated with OS and PFS.

**Results** Only patient’s age was prognostic for OS ( $p = 0.0037$ ) and PFS ( $p = 0.0088$ ). 23 PCNSL had the TSIC-shoulder, a middle-sized diameter ( $39.5 \pm 10.8$  mm), volume ( $15.7 \pm 11.3$  ml), peritumoral edema ( $23 \pm 8.7$  mm) and moderately increased  $rCBV_{mean}$  and  $rCBV_{max}$  ( $1.7 \pm 0.5$ ;  $3.9 \pm 1.2$ ). Seven PCNSL with the TSIC-shoulder presented a sun-like pattern (“ $rCBV$ -sun”) with a rim of marginally high  $rCBV$ . These unifocal PCNSL were larger ( $43 \pm 11.2$  mm;  $25.62 \pm 19.2$  ml), with more peritumoral edema ( $32.8 \pm 7.6$  mm) and lower  $CBV_{mean}$  ( $0.8 \pm 0.3$ ) and  $rCBV_{max}$  ( $2.2 \pm 0.7$ ), compared to the remaining six multifocal PCNSL without the TSIC-shoulder ( $26.3 \pm 8.3$  mm;  $4.7 \pm 4$  ml;  $16.3 \pm 6.4$  mm;  $2.4 \pm 1.6$ ;  $4.4 \pm 2.3$ ).

**Conclusions** Only patient age was predictive for OS and PFS of PCNSL; MR perfusion parameters and features were not. Most PCNSL revealed the TSIC-shoulder, moderate size, peritumoral edema and  $rCBV$  increase. However, larger, solitary PCNSL additionally had a  $rCBV$ -sun pattern and more edema, maybe due to a centrifugal vessel proliferation, whereas smaller, multifocal PCNSL contain apparently more concentrated and less permeable blood vessels represented by higher  $rCBV$ , no TSIC-shoulder and less edema.

**Keywords** Primary CNS lymphoma · MR perfusion ·  $rCBV$  · Overall survival · Progression-free survival · Prognostic value

## Introduction

Primary central nervous system lymphomas (PCNSL) affect more and more patients in our aging western population, but remain rare compared to other intracranial tumors such as glioblastomas [1–3]. The diagnosis of PCNSL is challenging because the MR morphology of PCNSL may imitate glioblastomas. However, differentiation of suspected PCNSL

from glioblastomas is of high clinical relevance, as their therapy strategies differ crucially and pre-surgical treatment of PCNSL with corticosteroids has to be avoided [4, 5]. MR perfusion techniques, such as the T2\*-weighted dynamic susceptibility contrast-enhanced (DSC)-perfusion, improve pre-surgical differentiation of PCNSL from glioblastomas. The regional cerebral blood volume ( $rCBV$ ) of the contrast-enhancing tumor normalized to the  $rCBV$  of the contralateral brain is a biomarker for neoangiogenesis in glioblastomas, correlating positively with the histological tumor grade [6–10] and negatively with the patients’ prognosis [11, 12].

In contrast to metastases, infiltrating glioblastomas are further characterized by a penumbral pattern of  $rCBV$  increase exceeding the central contrast-enhancing area [13–16]. PCNSL not only have an infiltrative growth pattern,

Stella Blasel and Rieke Vorwerk contributed equally as first authors to this work. Patrick N. Harter and Elke Hattingen contributed equally as senior authors to this work.

✉ Stella Blasel  
Stella.Blasel@kgu.de

Extended author information available on the last page of the article

but may also show a penumbral rCBV increase similar to glioblastomas [17, 18].

Further, it has been shown that rCBV in PCNSL is moderately increased to the contralateral brain, but still lower when compared to glioblastomas [17–26]. PCNSL may have a shoulder-like increase in the time–signal intensity curves (TSIC) at the end of the first passage of the contrast agent bolus through the microvasculature indicating moderate interstitial contrast agent leakage [17, 23, 24, 27–30]. This phenomenon is also known as the “TSIC-shoulder” [17].

The predictive value of these MR perfusion features for overall survival (OS) and progression-free survival (PFS) has not been investigated so far, being the aim of this retrospective study, together with other tumor and patient characteristics.

## Patients and methods

### Patients, first-line treatment and prognostic scores

We retrospectively selected all consecutive immunocompetent adult patients with PCNSL, who received a preoperative MRI examination including perfusion weighted images (PWI) with a T2\*-weighted technique, using dynamic susceptibility contrast-enhanced (DSC)-MRI, between 11/2009 and 07/2014. We excluded all tumors with large areas of necrosis on the T2-weighted images and only included PCNSL with homogenous contrast-enhancing lesions on T1-weighted images as characteristic MR imaging features of the majority of PCNSL in immunocompetent patients [31].

The local ethics committee approved this retrospective study. Patient consent form was waived by the ethics committee due to the retrospective design of the study. All MRI examinations followed clinical indications; no extra scans were performed for study reasons.

Histopathological diagnosis was based on stereotactical biopsies in all patients. Tumors were classified according to the World Health Organization (WHO) classification of brain tumors [32]. None of the patients had received treatment before the MRI examination.

Systemic immune-chemotherapy based on rituximab (R) and high-dose methotrexate (HDMTX) is the backbone of basic PCNSL therapy [33]. In our clinic, patients  $\geq 65$  years usually receive a first-line rituximab and high-dose methotrexate (R-HDMTX) based immune-chemotherapy [34, 35], whereas the younger patients or older patients in adequately good clinical condition undergo a sequential immune-chemotherapy with a R-HDMTX based induction therapy followed by a carmustine (BCNU) based intensified high-dose chemotherapy and autologous stem-cell transplantation (HDCT-ASCT) [36, 37]. For each patient, we assessed

the prognostic scores Karnofsky Performance Status (KPS), Eastern Co-operative of Oncology Group (ECOG), Memorial Sloan-Kettering Cancer Center (MSKCC) at tumor diagnosis.

### MR examination

MRI examination was performed at a 3T scanner (Verio; Siemens, Erlangen, Germany). PWI was performed with a T2\*-weighted technique, using DSC-MRI with a gradient-echo planar imaging sequence with 50 dynamic measurements (TR = 1880, TE = 30, flip angle 90°, FOV = 230 × 230 mm, matrix = 128 × 128, 3 mm slice thickness, 0.6 mm slice gap). Intravenous injection of 0.1 ml/kg Gadobutrol (1 M Gd-DO3A-butrol) using a power injector with a flow rate of 5 ml/s was followed by injection of a 20 ml bolus of 0.9% saline delivered at the same flow rate. The artery input function was defined in the middle cerebral artery of the diseased hemisphere. Thereafter, T1-weighted axial spin-echo sequence (TR = 600 ms, TE = 9 ms, FOV = 230 mm × 230 mm, matrix: 256 × 256, 3–4 mm slice thickness, 1 acquisition) was acquired as reference images using the same orientation and slice thickness as the PWI sequence.

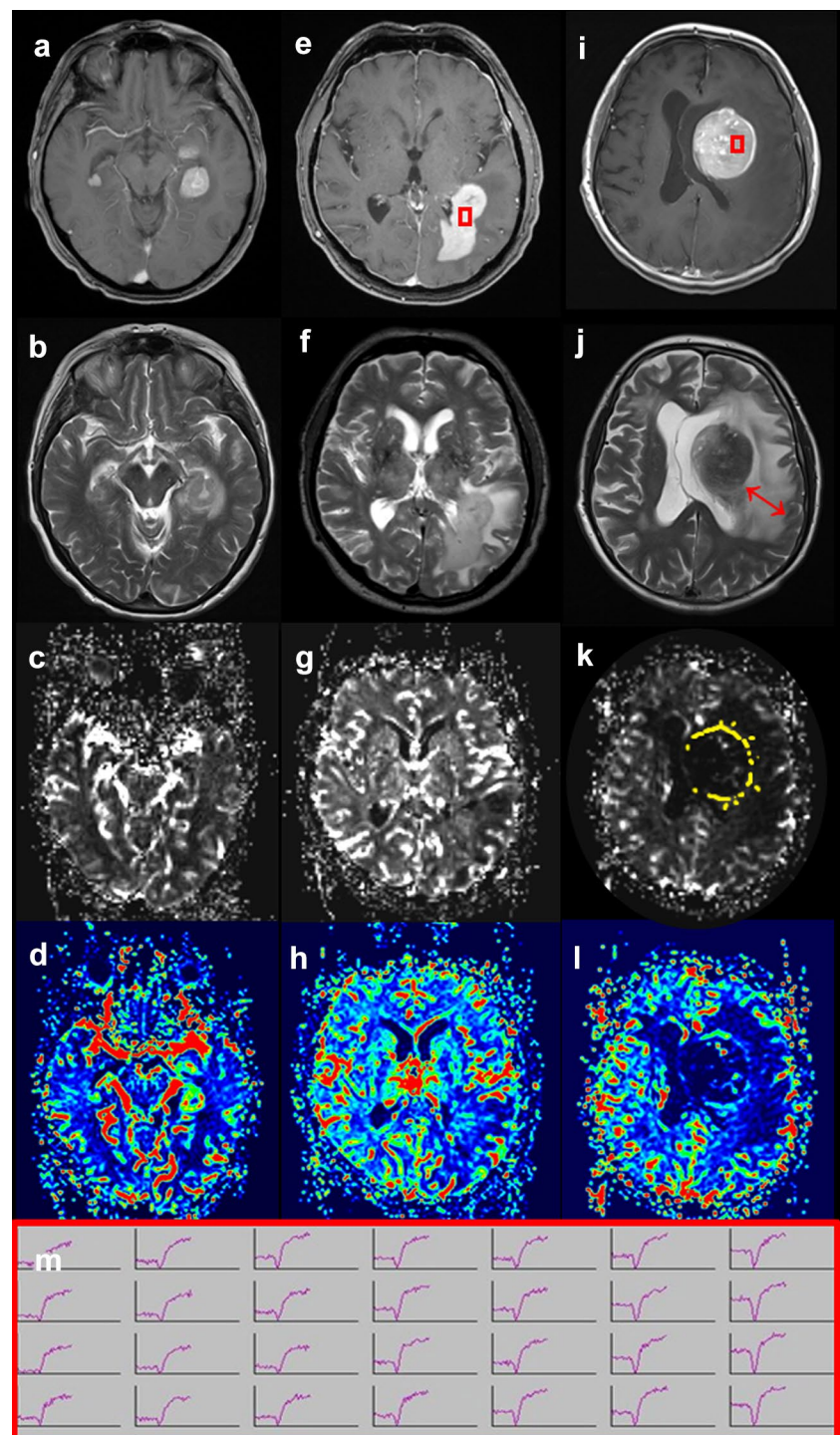
### PCNSL characteristics and morphology

We assessed the number of non-confluent PCNSL lesions, tumor size, volume and the peritumoral edema width as MR morphological parameters. Tumor size was measured (R.V., S.B.) by the maximal tumor diameter on the axial, sagittal and coronal plane on the contrast-enhanced T1-weighted sequence, depicting the solitary PCNSL or the biggest lesion of multifocal PCNSL. Further, we estimated the tumor volume according to the product of these three diameters divided by two (length × width × height/2) [38] and determined the width of peritumoral edema width in modification to Tung et al. [39] (Fig. 1).

### rCBV analysis

rCBV maps were generated with Syngo<sup>®</sup> Software (Siemens Medical Systems) featuring standard algorithms [40, 41] implemented at the MR scanner. The beginning and end of the first-pass bolus were determined through inspection of time–signal intensity curves (E.H., S.B.) with experience in interpreting dynamic perfusion images), and care was taken to exclude any recirculation-related signal. For rCBV calculations, only the area under the curve of the first-pass bolus was considered, as a simple measure to minimize the previously described confounding effects of contrast agent leakage [22].

**Fig. 1** Exemplary measurement of the peritumoral edema width as the maximal distance from the edge of PCNSL to the periphery of the surrounding hyperintense margin on the axial T2-weighted images (red arrowed line in **j**), the visually assessed MR perfusion pattern as “the rCBV-sun” (yellow streaks in **k**) and the typical MR perfusion feature named the “TSIC-Shoulder” with a baseline overshooting time–signal intensity curve (**e**, **i**, **m**). Exemplary case of each MR perfusion pattern subgroup with: Group 1 **a–d**: PCNSL without a TSIC-shoulder and without a rCBV-sun. Group 2 **e–h**: PCNSL with a TSIC-shoulder and without a rCBV-sun. Group 3 **i–l**: PCNSL with a TSIC-shoulder and with a rCBV-sun



Gray-coded rCBV maps were generated and aligned with the corresponding T1-weighted images to provide better visualization of tumor boundaries. First, we identified the contrast-enhancing tumor on the T1-weighted sequence. Then, we manually drew irregularly shaped ROIs (region of interests) covering the entire enhancing tumor on the rCBV parameter (R.V.). ROIs were carefully placed to exclude gray matter or vessels in each slice depicting the tumor,

by simultaneously reviewing the rCBV parameter map and the T1-weighted sequence that were linked to each other. After initial ROI measurements we performed a second-look analysis, thoroughly checking the first ROI placement and correcting any accidental ROI inclusion of cortical and vessel structures (R.V. and S.B.). We documented the average rCBV value ( $rCBV_{\text{mean}}$ ) and the maximal rCBV value ( $rCBV_{\text{max}}$ ) with their corresponding standard deviations.



These rCBV values were related to a standardized 30 mm<sup>2</sup> ROI in the normal-appearing white matter of the contralateral hemisphere. Hence, all rCBV values were expressed as normalized ratios. This approach has been shown to provide the best inter- and intraobserver reproducibility in previous studies [11, 42].

### TSIC-shoulder analysis

The signal intensity curves were generated and evaluated using the Syngo<sup>®</sup> Software (Siemens Medical Systems). We (R.V., S.B.) visually assessed, if signal recovery after the first pass signal drop exceeded baseline level which is defined as “TSIC-shoulder” (Fig. 1); and accordingly signal recovery to baseline or below baseline level was defined as absence of the TSIC-shoulder. Consequently, PCNSL were divided in “PCNSL with TSIC-shoulder” and “PCNSL without TSIC-shoulder”.

### Analysis of MR perfusion pattern: TSIC-shoulder and rCBV-sun

Reviewing the rCBV maps of the PCNSL, we visually recognized a new sun-like rCBV pattern in some PCNSL with a central decrease and a peripheral rCBV increase resembling sunbeams. We named this MRI perfusion pattern “rCBV-sun” according to its morphological resemblance (Fig. 1). The central parts of the rCBV-sun with decreased rCBV showed a homogenous enhancement on the equivalent contrast-enhanced T1-weighted images. Further, there were no visible matching necrotic areas on the corresponding T2-weighted images. Moreover, tumors with large visually delineable necrotic areas had been primarily excluded from the analysis.

In addition to the TSIC-shoulder, the PCNSL feature “PCNSL with rCBV-sun” respective “PCNSL without rCBV-sun” was also considered in the MR perfusion pattern analysis, defining three PCNSL subgroups (Fig. 1):

*Group 1* PCNSL without a TSIC-shoulder and without a rCBV-sun.

*Group 2* PCNSL with a TSIC-shoulder and without a rCBV-sun.

*Group 3* PCNSL with a TSIC-shoulder and with a rCBV-sun.

### Statistics, overall survival and progression-free survival analyses

Statistical analyses were performed using JMP 13.1 (SAS, Cary, North Carolina, USA) and BIAS<sup>™</sup> version 10.12 software (2014 Epsilon, Frankfurt, Germany) with a significance level of  $p < 0.05$ .

We assessed the date of death (DOD) or the date of last contact (censored patient`s) for statistical analysis of the overall survival (OS) of our patient cohort. Calculation of OS was started from the day of stereotactical biopsy [43].

Progression-free survival (PFS) was defined as the time from the day of stereotactical biopsy to first documentation of disease progression on imaging or death from lymphoma within 4 months. Patients that were at complete remission (CR) at the time point of data analysis were censored at their last visit [44].

Prognostic value of the tumor and patient associated data (tumor size, tumor volume, peritumoral edema width, rCBV<sub>mean</sub> and rCBV<sub>max</sub> values, patient age and sex, as well as KPS, ECOG and MSKCC) on OS and PFS was tested in univariate analyses by the Chi-squared test. For the differences of OS and PFS in the dichotomized patient cohort “PCNSL with TSIC-shoulder” and “PCNSL without TSIC-shoulder”, we performed a log-rank and Wilcoxon matched pairs, as well as a Kaplan–Meier analysis. Further, we performed a subgroup analysis of the MR perfusion features rCBV-sun and TSIC-shoulder using a Kruskal–Wallis test.

Statistical analysis of the three basic therapy groups (R-HDMTX, HDCT-ASCT, alternative therapy) in respect to their prognostic scores (age, KPS, ECOG, MSKCC) and MR perfusion parameters (MR perfusion subgroup, rCBV<sub>mean</sub> and rCBV<sub>max</sub>) was performed by a Kruskal–Wallis test. Further, PFS and OS Kaplan–Meier analyses of the three basic therapy regimes (R-HDMTX, HDCT-ASCT; alternative therapy) were performed.

## Results

### Patients, first-line treatment and prognostic scores

37 patients (18 female, 19 male) with histopathological approved PCNSL were included in the study with a mean age of  $64 \pm 11.2$  years ranging from 46 to 82 years. All 37 PCNSL were diffuse large B-cell lymphomas with the morphological variant of T-cell rich B-cell lymphomas in two of them. At the time point of OS analysis, 23 out of 37 patients (62%) were dead and 14 patients (38%) were censored at their last visit. Two patients with tumor progression were still alive at the time point of analysis and 12 patients were censored at CR for PFS analysis. Median OS and PFS was 664 days (21.8 months; range 34–2691 days) and 589 days (19 months; range 26–2691 days), respectively.

18 PCNSL patients showed singular solid contrast-enhancing tumors, 19 patients had multiple non-confluent solid PCNSL lesions (ranging from 2 to 10 lesions).

Patient age at PCNSL diagnosis was negatively associated with OS ( $p = 0.0037$ ) and PFS ( $p = 0.0088$ ), whereas the prognostic scores KPS, ECOG and MSKCC revealed no

statistically relevant effect on OS and PFS. Patient's sex was not predictive for the OS or PFS (Table 1).

Patients had different first-line therapeutic regimen. Eighteen patients received a first-line immune-chemotherapy based on R-HDMTX [34, 35], fourteen patients received HDCT-ASCT [36, 37] and five patients received alternative therapy concepts due to their poor clinical condition at PCNSL diagnosis [KPS of 38 (mean, range 20–50)] (Table 2). These patients received rituximab monotherapy ( $n = 1$ ), combined with whole brain radiation ( $n = 2$ ) or whole brain radiation therapy alone ( $n = 2$ ).

The HDCT-ASCT therapy concept revealed the longest PFS and OS, not even reaching the median PFS and median OS with more than half of the patients still alive and in CR at the time point of analysis. Therefore, PFS and OS of the patients following HDCT-ASCT basic therapy was longer compared to the R-HDMTX (median PFS 220 days and OS 320 days) and alternative therapy groups (median PSF 55 days and OS 157 days) with  $p < 0.001$  for each. PFS in the R-HDMTX group was significantly longer than in the group of patients with alternative therapy regimes ( $p < 0.05$ ) (Table 2, Fig. 2). However, age and prognostic scores (KPS, ECOG and MSKCC) also differed significantly between the three therapy concepts, whereas their MR perfusion parameters (proportion of MR perfusion subgroup  $rCBV_{\text{mean}}$  and  $rCBV_{\text{max}}$ ) did not (Table 2).

### PCNSL characteristics and morphology

MR morphological criteria (tumor volume and maximal diameter, number of tumor lesions, peritumoral edema width) were not predictive for the OS or PFS (Table 1).

### rCBV analysis

ROI based rCBV measurements of  $rCBV_{\text{mean}}$  and  $rCBV_{\text{max}}$  were performed in 36 of the 37 PCNSL patients. In one patient, the definition of the beginning and end of the first-pass bolus was not possible due to a flattened and broad first bolus drop and ergo rCBV establishment failed.

Compared to the reference ROI in the normal-appearing white matter  $rCBV_{\text{mean}}$  was increased in 30 out of the 36 PCNSL patients with rCBV measurements (= 83%) (mean  $1.67 \pm 0.9$  ranging from 0.05 to 4.12) and  $rCBV_{\text{max}}$  was increased in 34 of all 36 PCNSL patients (mean  $3.69 \pm 1.54$ , ranging from 0.94 to 7.55) with rCBV measurements. Neither  $rCBV_{\text{mean}}$  nor  $rCBV_{\text{max}}$  was predictive for the OS or PFS (Table 1).

### TSIC-shoulder analysis

The analysis of the TSIC curve in respect to the appearance or absence of the TSIC-shoulder was possible in all 37 patients. The TSIC-shoulder was found in 31 out of all 37 patients (84%) and there were six PCNSL without a TSIC-shoulder.

The OS and PFS revealed no significant differences between the patient subgroups “PCNSL with a TSIC-shoulder” vs. “PCNSL without a TSIC-shoulder” with a median OS of 930 days vs. 664 days and with  $p = 0.5108/0.522$  (log-rank/Wilcoxon) and a median PFS of 987 vs. 347 days and with  $p = 0.3618/0.4104$  (Fig. 2).

**Table 1** Tumor and patient associated PCNSL criteria at diagnosis and their effect on the overall survival and progression-free survival

Parameter	Mean $\pm$ SD (range)	OS <i>p</i> value	PFS <i>p</i> value
Patient age [years]	64 $\pm$ 11.2 (46–82)	$p = 0.0037^*$	$p = 0.0088^*$
Sex (female/male)	18/19	$p = 0.5574$	$p = 0.6693$
KPS	61 $\pm$ 16.5 (20–90)	$p = 0.1027$	$p = 0.4075$
ECOG	1.8 $\pm$ 1 (0–4)	$p = 0.2087$	$p = 0.5518$
MSKCC	2.3 $\pm$ 0.7 (1–3)	$p = 0.073$	$p = 0.0734$
Tumor volume [ml]	15.7 $\pm$ 13.4 (0.7–62.3)	$p = 0.7922$	$p = 0.7583$
Tumor size [mm]	37.9 $\pm$ 11.4 (16.9–64.1)	$p = 0.9571$	$p = 0.8964$
Number of lesions	3.4 $\pm$ 3.4 (1–10)	$p = 0.7019$	$p = 0.3548$
$rCBV_{\text{mean}}$	1.67 $\pm$ 0.9 (0.05–4.12)	$p = 0.5515$	$p = 0.5184$
$rCBV_{\text{max}}$	3.69 $\pm$ 1.54 (0.94–7.55)	$p = 0.4674$	$p = 0.3778$
Peritumoral edema [mm]	24.4 $\pm$ 9.9 (6.5–44.9)	$p = 0.4018$	$p = 0.266$

PCNSL primary CNS lymphoma, OS overall survival, PFS progression-free survival, SD standard deviation, KPS Karnofsky Performance Status, ECOG Eastern Co-operative of Oncology Group, MSKCC Memorial Sloan-Kettering Cancer Center

\* Significant with  $p < 0.05$ , rCBV regional cerebral blood volume

**Table 2** Clinical data and prognostic scores of first-line treatment in correlation to their MR perfusion parameters

	Group 1 (R-HDMTX)	Group 2 (HDCT-ASCT)	Group 3 (alternative therapy)	<i>p</i> value
Total number of patients ( <i>n</i> )	18	14	5	
MR perfusion subgroup I ( <i>n</i> )	3	3	0	1 vs. 2: <i>p</i> = 0.7408
MR perfusion subgroup II ( <i>n</i> )	12	9	3	1 vs. 3: <i>p</i> = 0.4263
MR perfusion subgroup III ( <i>n</i> )	3	2	2	2 vs. 3: <i>p</i> = 0.4157
Age [years] (mean ± SD) (range)	69 ± 10 (47–79)	56 ± 7 (46–68)	66 ± 15 (50–82)	1 vs. 2: <i>p</i> = 0.0021** 1 vs. 3: <i>p</i> = 0.6612 2 vs. 3: <i>p</i> = 0.0765
KPS (mean ± SD) (range)	65 ± 15.4 (40–90)	64.3 ± 12.8 (40–80)	38 ± 11 (20–50)	1 vs. 2: <i>p</i> = 0.858 1 vs. 3: <i>p</i> = 0.0057** 2 vs. 3: <i>p</i> = 0.0069**
ECOG (mean ± SD) (range)	1.5 ± 0.9 (0–3)	1.6 ± 0.6 (1–3)	3 ± 0.7 (2–4)	1 vs. 2: <i>p</i> = 0.509 1 vs. 3: <i>p</i> = 0.0038** 2 vs. 3: <i>p</i> = 0.0114*
MSKCC score (mean) range	2 (1–3)	2 (1–3)	3 (3)	1 vs. 2: <i>p</i> = 0.6442 1 vs. 3: <i>p</i> = 0.0526 2 vs. 3: <i>p</i> = 0.0439*
rCBV <sub>mean</sub> (mean ± SD) (range)	1.6 ± 0.9 (0.05–4.0)	1.9 ± 1.0 (2.7–4.1)	1.1 ± 0.4 (0.7–1.5)	1 vs. 2; <i>p</i> = 0.4506 1 vs. 3; <i>p</i> = 0.4506 2 vs. 3; <i>p</i> = 0.1505
rCBV <sub>max</sub> (mean ± SD) (range)	3.5 ± 1.6 (0.9–7.3)	4.2 ± 1.5 (2.2–7.6)	2.9 ± 1.2 (1–3.9)	1 vs. 2; <i>p</i> = 0.2272 1 vs. 3; <i>p</i> = 0.5462 2 vs. 3; <i>p</i> = 0.2271
Median PFS (range) [days] Deceased or recurrent/censored at CR	220 (46–2303) 17/1	– 3/11	55 (26–273) 5/0	1 vs. 2; <i>p</i> < 0.001** 1 vs. 3; <i>p</i> = 0.0193* 2 vs. 3; <i>p</i> < 0.001**
Median OS (range) [days] Deceased/alive	319.5 (48–2407) 15/3	– 3/11	157 (47–425) 5/0	1 vs. 2; <i>p</i> < 0.001** 1 vs. 3; <i>p</i> = 0.0659 2 vs. 3; <i>p</i> < 0.001**

R-HDMTX rituximab and high-dose methotrexate immune-chemotherapy, HDCT high-dose chemotherapy, ASCT autologous stem-cell transplantation, TSIC time–signal intensity curve, SD standard deviation, DLBL Diffuse large cell B-cell lymphoma, rCBV regional cerebral blood volume, KPS Karnofsky Performance Status, ECOG Eastern Co-operative of Oncology Group, MSKCC Memorial Sloan-Kettering Cancer Center, PFS progression-free survival, OS overall survival, CR complete remission

\* Significant with *p* < 0.05 and with \*\* *p* < 0.01

### Analysis of MR perfusion pattern: TSIC-shoulder and rCBV-sun

Measurements of rCBV were possible in 36 out of all 37 patients. For statistical analysis and comparison of the MR perfusion pattern subgroups, the patient without measurable rCBV values was excluded (*n* = 36).

The majority of PCNSL belonged to the subgroup of PCNSL with the TSIC-shoulder and no rCBV-sun (group 2; *n* = 23, Figs. 1, 3, Table 3). They were further characterized by middle tumor sizes, volumes and peritumoral edema widths, as well as moderately increased rCBV values (Table 3, Figs. 1, 3).

The other two PCNSL-MR perfusion pattern subgroups were fewer and differed in tumor sizes and peritumoral edema widths.

The PCNSL with the TSIC-shoulder and the rCBV-sun (group 3; *n* = 7, Figs. 1, 3, Table 3) were larger tumors than

the PCNSL without the TSIC-shoulder and no rCBV-sun (group 1; *n* = 6, Figs. 1, 3, Table 3). In addition, they were surrounded by larger peritumoral edema rim and had significant lower rCBV values (Table 3, Figs. 1, 3). Comparison of the number of lesions of group 3 vs. group 1 revealed a higher lesion load in the latter (6 vs. 1; *p* = 0.0043, Table 3 and Figs. 1, 3). Correlation of OS and PFS analyses between the three MR perfusion pattern subgroups was not possible due to their small sample sizes (Table 3).

### Discussion

In contrast to glioblastomas, PCNSL are not hypervascular tumors. Since rCBV values correspond to the microvessel density [45], neoangiogenesis in glioblastomas is reflected by marked rCBV increases [46]. Although neoangiogenesis is absent or only marginal in PCNSL [47–49], PCNSL

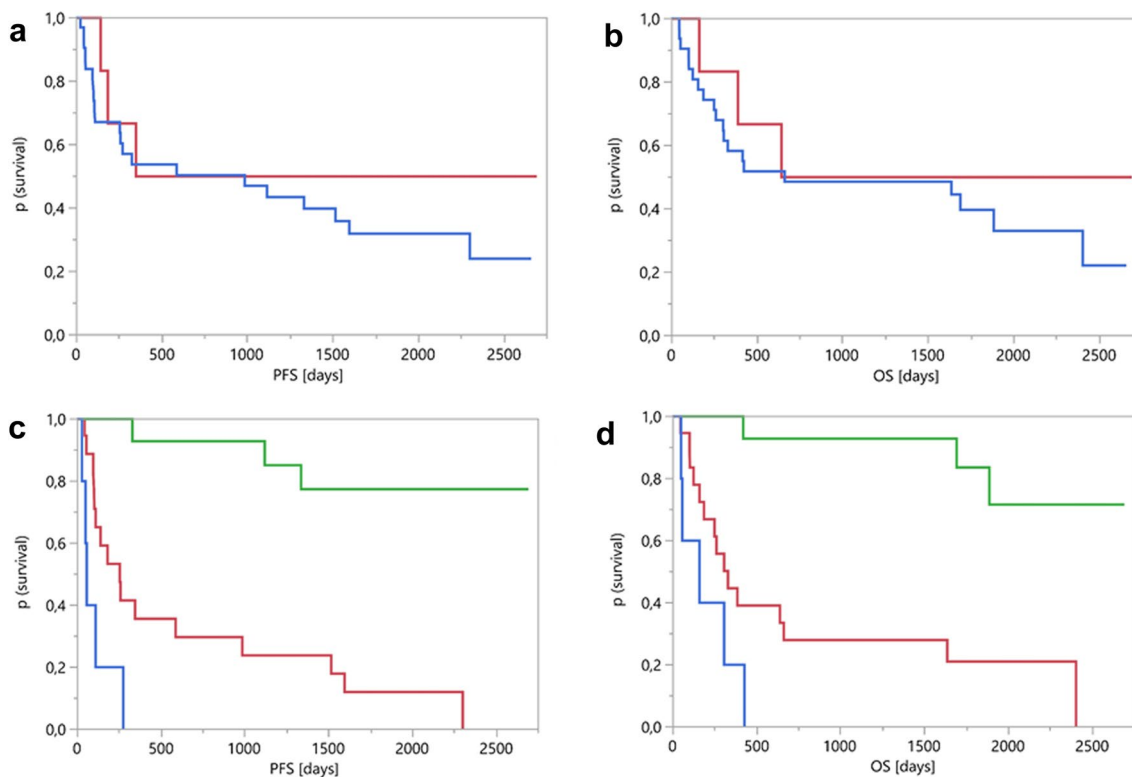


**Fig. 2** Kaplan–Meier analysis shows **a** no statistical PFS differences comparing “PCNSL with the TSIC-shoulder” (blue curve) with “PCNSL without the TSIC-Shoulder” (red curve); **b** no statistical OS differences comparing “PCNSL with the TSIC-shoulder” (blue curve) with “PCNSL without the TSIC-shoulder” (red curve); **c** significantly longer PFS in the PCNSL patients following HDCT-ASCT first-line

therapy (green curve), compared to the patients with R-HDMTX basic therapy (red curve) and alternative therapy (blue curve); **d** significantly longer OS in the PCNSL patients following HDCT-ASCT first-line therapy (green curve), compared to the patients with R-HDMTX basic therapy (red curve) and alternative therapy (blue curve)

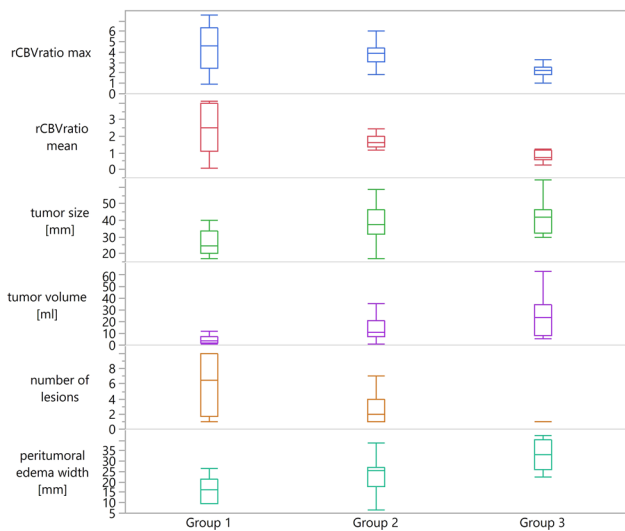


**Fig. 3** Boxplots summarizing significant differences of tumor-associated data of the MR perfusion pattern subgroups

also seem to interact with the vasculature of the brain, since PCNSL usually present with moderately increased rCBV values [17, 18, 20–26, 28, 29, 50, 51]. However, the prognostic effect of rCBV in PCNSL remains obscure and rCBV pattern analysis has not yet been performed.

PCNSL may show a characteristic time–signal intensity curve in MR perfusion known as the TSIC-shoulder [17]. This phenomenon was explained by moderate vessel permeability causing a late interstitial accumulation of contrast agent [17, 18, 23, 24, 27–30, 51] that is thought to induce T1-shortening effects with a shoulder-like increase at the end of the time–signal intensity curve. This hemodynamic feature is typical for PCNSL [24], whereas the immediate interstitial extravasation of contrast agent in glioblastomas occurs during the first signal drop [17]. However, the predictive value of the TSIC-shoulder on OS and PFS in PCNSL has not been investigated so far.

In the current study, we could confirm that the TSIC-shoulder appears in the majority of PCNSL, but the presence of the TSIC-shoulder in PCNSL was neither predictive for OS nor for PFS. In fact, besides patient age at PCNSL diagnosis, no other evaluated patient or tumor

**Table 3** Patient and tumor associated PCNSL criteria of the MR perfusion pattern subgroup analysis

	Group 1	Group 2	Group 3	<i>p</i> value
TSIC-shoulder	No	Yes	Yes	
rCBV-sun	No	No	Yes	
Age [years] (mean ± SD) (range)	65 ± 5 (59–74)	61 ± 12 (46–77)	71 ± 10 (52–82)	1 vs. 2: <i>p</i> = 0.54 1 vs. 3: <i>p</i> = 0.46 2 vs. 3: <i>p</i> = 0.098
DLBL ( <i>n</i> )	5	22	7	
T-cell rich ( <i>n</i> )	1	1	0	
Peritumoral edema width [mm] (mean ± SD) (range)	16.3 ± 6.4 (9.5–26.5)	23 ± 8.7 (6.5–39.1)	32.8 ± 7.6 (22.5–42.6)	1 vs. 2; <i>p</i> = 0.0965 1 vs. 3; <i>p</i> = 0.0047** 2 vs. 3; <i>p</i> = 0.0263*
Tumor volume [ml] (mean ± SD) (range)	4.7 ± 4 (0.7–12.2)	15.7 ± 11.3 (1.7–44.8)	25.6 ± 19.2 (5.2–62.3)	1 vs. 2; <i>p</i> = 0.0166* 1 vs. 3; <i>p</i> = 0.0072* 2 vs. 3; <i>p</i> = 0.2191
Tumor size [mm] (mean ± SD)	26.3 ± 8.3 (16.9–40.3)	39.5 ± 10.8 (17.1–58.7)	43 ± 11.2 (29.9–64.1)	1 vs. 2; <i>p</i> = 0.0207* 1 vs. 3; <i>p</i> = 0.0207* 2 vs. 3; <i>p</i> = 0.4328
Mean number of lesions (range)	6 (1–10)	3 (1–10)	1 (1)	1 vs. 2; <i>p</i> = 0.0884 1 vs. 3; <i>p</i> = 0.0043** 2 vs. 3; <i>p</i> = 0.0263*
rCBV <sub>mean</sub> (mean ± SD) (range)	2.4 ± 1.6 (0.1–4.1)	1.7 ± 0.5 (1.2–3.2)	0.8 ± 0.3 (0.3–1.2)	1 vs. 2; <i>p</i> = 0.4188 1 vs. 3; <i>p</i> = 0.0007** 2 vs. 3; <i>p</i> = 0.0005**
rCBV <sub>max</sub> (mean ± SD) (range)	4.4 ± 2.3 (0.9–7.6)	3.9 ± 1.2 (1.8–7.3)	2.2 ± 0.7 (1–3.3)	1 vs. 2; <i>p</i> = 0.5975 1 vs. 3; <i>p</i> = 0.0049** 2 vs. 3; <i>p</i> = 0.0026*
Median PFS (range) [days]	– (161–2691)	300 (26–2617)	1682 (55–2662)	
Deceased or recurrent/censored at CR	3/3	17/6	4/3	
Median OS (range) [days]	– (161–2691)	418 (47–2617)	1682 (55–2662)	
Deceased/alive	3/3	15/8	4/3	

PCNSL primary CNS lymphoma, TSIC time–signal intensity curve, SD standard deviation, DLBL Diffuse large cell B-cell lymphoma, OS overall survival, rCBV regional cerebral blood volume, PFS progression-free survival, CR complete remission

\* Significant with *p* < 0.05 and with \*\* *p* < 0.01

related parameter (sex, number of lesions, tumor size, peritumoral edema width, rCBV<sub>mean</sub> and rCBV<sub>max</sub> values, ECOG, KPS, MSKCC) was associated with the OS and PFS time in PCNSL patients. In accordance with previous studies, age was negatively correlated with OS of PCNSL patients [43, 52, 53].

We also considered first-line therapy into our prognostic analysis, revealing longer OS and PFS in the group of patients receiving intensified HDCT-ASCT therapy, compared to the group of patients with R-HDMTX based immune-chemotherapy alone or alternative therapeutic concepts at first sight. However, when comparing the age and KPS structure of the three patient groups, it is evident that these prognostic differences rather seem to be an effect of patient age and/or their clinical status at PCNSL diagnosis. Interestingly, MR perfusion parameters did not differ between the three therapy regimens as another hint they do not seem to influence prognosis of PCNSL patients.

Valles et al. [54] also found various CBV levels in PCNSL. In contrast to our results, they found patients having PCNSL with higher rCBV values had a longer OS and PFS. The authors discussed that the shorter OS and PFS in patients having PCNSL with lower rCBV may be caused by a hypoxic microvessel environment decreasing the delivery of intravenous chemotherapeutics to the tumor.

In the current study, we observed different MR perfusion patterns in relation to the tumor morphology, the tumor sizes and widths of peritumoral edema. Further, we noticed different MR perfusion characteristics in multifocal and solitary PCNSL. The majority of solitary PCNSL revealed the TSIC-shoulder, moderately increased rCBV values and a moderate size of tumor and peritumoral edema rim. During our analysis, we visually recognized a new “rCBV-sun” pattern in the rCBV maps of a small number of PCNSL. The rCBV-sun describes PCNSL with centrally lowered rCBV values and a sunbeam-like rCBV increase at the tumor margin of the contrast-enhancing tumor area. This pattern was exclusively



found in PCNSL with the TSIC-shoulder and characterized larger tumors with larger peritumoral edema rims and lower rCBV values measured in the entire contrast-enhancing tumor region. In contrast, small-sized multifocal PCNSL were characterized by the absence of the TSIC-shoulder and the rCBV-sun. Further, they revealed small edema rims and relatively high measured rCBV values.

Hence, the PCNSL with a TSIC-shoulder and the rCBV-sun should represent relatively avascular lesions, whereas the PCNSL without a TSIC-shoulder should be lesions with a relatively high microvessel density. During the manual ROI based rCBV analysis, we put special effort on sparing gray matter and vessels by simultaneously inspecting the contrast-enhanced T1-weighted images. Therefore, we assume that the marginal sunbeam-like rCBV increase of the rCBV-sun reflects changes of the microvasculature.

Further, there were no visible signs of tumor necrosis in the central area of the rCBV reduction in the corresponding T2- or contrast-enhanced T1-weighted images. In addition, we can exclude therapy influences on MR morphology and perfusion pattern of our PCNSL, since MRI and DSC-perfusion were performed before surgery and before the application of corticosteroids or any other drugs affecting the blood–brain barrier.

Instead of performing true neoangiogenesis with active vessel sprouting such as gliomas, PCNSL infiltrate the brain by a characteristic angiocentric growth pattern, in which the tumor cells cluster around the pre-existing vessels of the brain [55]. The marginally pronounced rCBV increase in PCNSL might at least partially indicate reactive changes of these infiltrative “tumor-cuffs” with the centrally encased non-neoplastic vasculature of the brain. Indeed like in inflammation, a slight increase of the vasculature with microvascular proliferations has been found in PCNSL [56–59]. Therefore, we suppose that rCBV increase in PCNSL is mainly caused by immunoreactive changes of the normal brain vasculature against the infiltrating lymphoma cells. These tumor-vascular interactions would be bound to the border zones of the tumor and the adjacent vessels of the normal brain tissue. In larger PCNSL, these reactive “fighting front” would form of a marginal ring-like wall leading to the MR pattern of the rCBV-sun with a net  $rCBV_{\text{mean}}$  and  $rCBV_{\text{max}}$  decrease, whereas in smaller PCNSL, the entire tumor mass would become part of this reactive zone, causing more profoundly increased rCBV values.

These tumor-vascular interactions might simultaneously activate immunoreactive pathways. However, these activations might also be dependent on additional factors, e.g., composition of the extracellular matrix (ECM). A previous study already suggested that appearance of the TSIC-shoulder might be associated with a less dense matrix of perivascular reticulin fibers [17]. In fact, a loosened matrix in PCNSL with a TSIC-shoulder could enable

more immunoreactive cascades than in PCNSL without a TSIC-shoulder and a hypothetically denser ECM. Therefore, enlargement of the tumor and its surrounding edema could be triggered in PCNSL with the TSIC-shoulder and rather restricted in PCNSL without a TSIC-shoulder in correlation to the strengths of their immune response.

Apart from indicating dynamics of interstitial contrast media leakage, the absence or presence of the TSIC-shoulder might also hint to differences in the composition of the blood–brain barrier of the microvasculature in PCNSL. The signal intensity increase resulting in the TSIC-shoulder is thought to be caused by the shortening of T1-relaxation time due to contrast agent that crosses the disrupted blood–brain barrier [24]. Finally, a higher density of less permeable microvessels in a denser ECM in PCNSL without the TSIC-shoulder may lead to higher rCBV, smaller tumors and peritumoral edema rims.

## Limitations

The main limitation of this study is the retrospective analysis of a limited sample size.

The retrospective approach allowed us to collect an statistically acceptable number of PCNSL patients from a single center, but the three groups of PCNSL defined by different morphology and MR perfusion pattern were yet too small to be analyzed with regard to OS and PFS.

Further, we did not the extent of the PCNSL disease with potential ocular or CSF dissemination in our OS and PFS analysis, since these scopes were beyond the focus of this investigation.

Unfortunately, we were unable to perform a distinct histopathological correlation of the MR perfusion phenomena found due to the small PCNSL specimen gained through stereotactical biopsy and the retrospective setting of the current work. Thus, all discussed MR histopathological relationships remain hypothetical and should be investigated in future prospective neuro-oncological multicenter trials. Future studies should, moreover, analyze if the different groups of PCNSL that we defined herein also indicate distinct histopathological subtypes.

Furthermore, T1-shortening effects were not corrected, i.e., by pre-injection of contrast agent. Therefore, rCBV values of our study are subjected to be underestimated [22, 60, 61]. However, pre-injection method might influence the shoulder-like time–signal intensity increase, so that this method may have disadvantages analyzing PCNSL.

Finally, we did not perform computed coregistration and alignment of the contrast-enhanced MR perfusion with the T1-weighted sequences, i.e., by FSL software [62]. Instead all ROIs were manually placed on the gray-coded-rCBV parameter maps linked to the equivalent T1-weighted image,

trying to visually exclude necrotic areas, cortex and vessel structures as a more practical but imprecise way of rCBV assessment in the daily routine.

## Conclusions

Only patient age was prognostic for the OS and PFS of PCNSL patients, whereas diversified MR perfusion features were not. Most PCNSL were characterized by the TSIC-shoulder, middle sizes of the tumor and peritumoral edema and moderately increased rCBV values.

Two minor groups of PCNSL were found with differing rCBV pattern, tumor sizes and number of lesions:

1. Unifocal huge tumors with large edema rims and a “the rCBV-sun” as a new MR perfusion pattern describing marginal (sunbeam-like) rCBV increase around a central rCBV decrease, possibly indicating centrifugal vessel proliferations.
2. Multifocal small PCNSL with higher rCBV values, small peritumoral edema rims and no TSIC-shoulder, possibly indicating a higher density of less permeable microvasculature.

These MR morphological and MR perfusion differences might possibly reflect various biological subtypes of PCNSL, but seem to have no prognostic impact.

**Acknowledgements** M.M. would like to thank the Luxembourg National Research Fond (FNR) for the support (FNR PEARL P16/BM/11192868 Grant).

**Funding** The study was not funded by external sources.

## Compliance with ethical standards

**Conflicts of interest** The authors declared that they have no conflict of interest.

**Ethical standard statement** This study was approved by the institutional review board at Frankfurt Goethe University and was performed in accordance with the ethical standards for human subjects research. For this type of study formal consent is not required.


## References

1. Olson JE, Janney CA, Rao RD et al (2002) The continuing increase in the incidence of primary central nervous system non-Hodgkin lymphoma: a surveillance, epidemiology, and end results analysis. *Cancer* 95:1504–1510
2. Dolecek TA, Propp JM, Stroup NE, Kruchko C (2012) CBTRUS statistical report: primary brain and central nervous system tumors diagnosed in the United States in 2005–2009. *Neuro Oncol* 14(Suppl 5):v1–v49. <https://doi.org/10.1093/neuonc/nos218>
3. O’Neill BP, Decker PA, Tieu C, Cerhan JR (2013) The changing incidence of primary central nervous system lymphoma is driven primarily by the changing incidence in young and middle-aged men and differs from time trends in systemic diffuse large B-cell non-Hodgkin’s lymphoma. *Am J Hematol* 88:997–1000. <https://doi.org/10.1002/ajh.23551>
4. Schlegel U (2009) Primary CNS lymphoma. *Ther Adv Neurol Disord* 2:93–104. <https://doi.org/10.1177/1756285608101222>
5. Grommes C, DeAngelis LM (2017) Primary CNS Lymphoma. *J Clin Oncol Off J Am Soc Clin Oncol* 35:2410–2418. <https://doi.org/10.1200/JCO.2017.72.7602>
6. Aronen HJ, Gazit IE, Louis DN et al (1994) Cerebral blood volume maps of gliomas: comparison with tumor grade and histologic findings. *Radiology* 191:41–51
7. Chaudhry IH, O’Donovan DG, Brenchley PE et al (2001) Vascular endothelial growth factor expression correlates with tumour grade and vascularity in gliomas. *Histopathology* 39:409–415
8. Lee SJ, Kim JH, Kim YM et al (2001) Perfusion MR imaging in gliomas: comparison with histologic tumor grade. *Korean J Radiol* 2:1–7
9. Cha S (2004) Perfusion MR imaging of brain tumors. *Top Magn Reson Imaging* 15:279–289
10. Law M, Yang S, Babb JS et al (2004) Comparison of cerebral blood volume and vascular permeability from dynamic susceptibility contrast-enhanced perfusion MR imaging with glioma grade. *AJNR Am J Neuroradiol* 25:746–755
11. Law M, Young RJ, Babb JS et al (2008) Gliomas: predicting time to progression or survival with cerebral blood volume measurements at dynamic susceptibility-weighted contrast-enhanced perfusion MR imaging. *Radiology* 247:490–498
12. Jabehdar Maralani P, Melhem ER, Wang S et al (2015) Association of dynamic susceptibility contrast-enhanced MR Perfusion parameters with prognosis in elderly patients with glioblastomas. *Eur Radiol* 25:2738–2744. <https://doi.org/10.1007/s00330-015-3640-4>
13. Blasel S, Franz K, Ackermann H et al (2011) Stripe-like increase of rCBV beyond the visible border of glioblastomas: site of tumor infiltration growing after neurosurgery. *J Neurooncol* 103:575–584
14. Blasel S, Franz K, Mittelbronn M et al (2010) The striate sign: peritumoral perfusion pattern of infiltrative primary and recurrence gliomas. *Neurosurg Rev* 33:193–204
15. Chiang IC, Kuo YT, Lu CY et al (2004) Distinction between high-grade gliomas and solitary metastases using peritumoral 3-T magnetic resonance spectroscopy, diffusion, and perfusion imagings. *Neuroradiology* 46:619–627
16. Law M, Cha S, Knopp EA et al (2002) High-grade gliomas and solitary metastases: differentiation by using perfusion and proton spectroscopic MR imaging. *Radiology* 222:715–721
17. Blasel S, Jurcoane A, Bähr O et al (2013) MR perfusion in and around the contrast-enhancement of primary CNS lymphomas. *J Neurooncol* 114:127–134
18. Rollin N, Guyotat J, Streichenberger N et al (2006) Clinical relevance of diffusion and perfusion magnetic resonance imaging in assessing intra-axial brain tumors. *Neuroradiology* 48:150–159
19. Hakyemez B, Erdogan C, Bolca N et al (2006) Evaluation of different cerebral mass lesions by perfusion-weighted MR imaging. *J Magn Reson Imaging* 24:817–824
20. Lee IH, Kim ST, Kim HJ et al (2010) Analysis of perfusion weighted image of CNS lymphoma. *Eur J Radiol* 76:48–51
21. Calli C, Kitis O, Yuntun N et al (2006) Perfusion and diffusion MR imaging in enhancing malignant cerebral tumors. *Eur J Radiol* 58:394–403
22. Cha S, Knopp EA, Johnson G et al (2002) Intracranial mass lesions: dynamic contrast-enhanced susceptibility-weighted echo-planar perfusion MR imaging. *Radiology* 223:11–29

23. Hartmann M, Heiland S, Harting I et al (2003) Distinguishing of primary cerebral lymphoma from high-grade glioma with perfusion-weighted magnetic resonance imaging. *Neurosci Lett* 338:119–122
24. Liao W, Liu Y, Wang X et al (2009) Differentiation of primary central nervous system lymphoma and high-grade glioma with dynamic susceptibility contrast-enhanced perfusion magnetic resonance imaging. *Acta Radiol* 50:217–225
25. Sugahara T, Korogi Y, Shigematsu Y et al (1999) Perfusion-sensitive MRI of cerebral lymphomas: a preliminary report. *J Comput Assist Tomogr* 23:232–237
26. Kickingereder P, Wiestler B, Sahm F et al (2014) Primary central nervous system lymphoma and atypical glioblastoma: multiparametric differentiation by using diffusion-, perfusion-, and susceptibility-weighted MR imaging. *Radiology* 272:843–850. <https://doi.org/10.1148/radiol.14132740>
27. Wang S, Kim S, Chawla S et al (2011) Differentiation between glioblastomas, solitary brain metastases, and primary cerebral lymphomas using diffusion tensor and dynamic susceptibility contrast-enhanced MR imaging. *AJNR Am J Neuroradiol* 32:507–514. <https://doi.org/10.3174/ajnr.A2333>
28. Toh CH, Wei K-C, Chang C-N et al (2013) Differentiation of primary central nervous system lymphomas and glioblastomas: comparisons of diagnostic performance of dynamic susceptibility contrast-enhanced perfusion MR imaging without and with contrast-leakage correction. *AJNR Am J Neuroradiol* 34:1145–1149. <https://doi.org/10.3174/ajnr.A3383>
29. Nakajima S, Okada T, Yamamoto A et al (2015) Primary central nervous system lymphoma and glioblastoma: differentiation using dynamic susceptibility-contrast perfusion-weighted imaging, diffusion-weighted imaging, and (18)F-fluorodeoxyglucose positron emission tomography. *Clin Imaging* 39:390–395. <https://doi.org/10.1016/j.clinimag.2014.12.002>
30. Mangla R, Kolar B, Zhu T et al (2011) Percentage signal recovery derived from MR dynamic susceptibility contrast imaging is useful to differentiate common enhancing malignant lesions of the brain. *AJNR Am J Neuroradiol* 32:1004–1010
31. Küker W, Nägele T, Korfel A et al (2005) Primary central nervous system lymphomas (PCNSL): MRI features at presentation in 100 patients. *J Neurooncol* 72:169–177. <https://doi.org/10.1007/s11060-004-3390-7>
32. Louis DN, Ohgaki H, Wiestler OD et al (2007) The 2007 WHO classification of tumours of the central nervous system. *Acta Neuropathol* 114:97–109
33. Schlegel U, Illerhaus G (2015) Leitlinien für Diagnostik und Therapie in der Neurologie: Primäre ZNS-Lymphome (PZNSL). <https://www.dgn.org/leitlinien/2984-ll-78-primaeere-zns-lymphome-pznsll>. Accessed 13 Dec 2017
34. Fritsch K, Kasenda B, Schorb E et al (2017) High-dose methotrexate-based immuno-chemotherapy for elderly primary CNS lymphoma patients (PRIMAINE study). *Leukemia* 31:846–852. <https://doi.org/10.1038/leu.2016.334>
35. Fritsch K, Kasenda B, Hader C et al (2011) Immunochemotherapy with rituximab, methotrexate, procarbazine, and lomustine for primary CNS lymphoma (PCNSL) in the elderly. *Ann Oncol* 22:2080–2085. <https://doi.org/10.1093/annonc/mdq712>
36. Illerhaus G, Müller F, Feuerhake F et al (2008) High-dose chemotherapy and autologous stem-cell transplantation without consolidating radiotherapy as first-line treatment for primary lymphoma of the central nervous system. *Haematologica* 93:147–148. <https://doi.org/10.3324/haematol.11771>
37. Ferreri AJM, Cwynarski K, Pulczynski E et al (2016) Chemioimmunotherapy with methotrexate, cytarabine, thiotepa, and rituximab (MATRix regimen) in patients with primary CNS lymphoma: results of the first randomisation of the International Extranodal Lymphoma Study Group-32 (IELSG32) phase 2 trial. *Lancet Haematol* 3:e217–e227. [https://doi.org/10.1016/S2352-3026\(16\)00036-3](https://doi.org/10.1016/S2352-3026(16)00036-3)
38. Patel TR, McHugh BJ, Bi WL et al (2011) A comprehensive review of MR imaging changes following radiosurgery to 500 brain metastases. *AJNR Am J Neuroradiol* 32:1885–1892. <https://doi.org/10.3174/ajnr.A2668>
39. Tung GA, Julius BD, Rogg JM (2003) MRI of intracerebral hematoma: value of vasogenic edema ratio for predicting the cause. *Neuroradiology* 45:357–362. <https://doi.org/10.1007/s00234-003-0994-0>
40. Rosen BR, Belliveau JW, Vevea JM, Brady TJ (1990) Perfusion imaging with NMR contrast agents. *Magn Reson Med* 14:249–265
41. Ostergaard L, Weisskoff RM, Chesler DA et al (1996) High resolution measurement of cerebral blood flow using intravascular tracer bolus passages. Part I: mathematical approach and statistical analysis. *Magn Reson Med* 36:715–725
42. Lev MH, Rosen BR (1999) Clinical applications of intracranial perfusion MR imaging. *Neuroimaging Clin N Am* 9:309–331
43. Abrey LE, Ben-Porat L, Panageas KS et al (2006) Primary central nervous system lymphoma: the Memorial Sloan-Kettering Cancer Center prognostic model. *J Clin Oncol Off J Am Soc Clin Oncol* 24:5711–5715. <https://doi.org/10.1200/JCO.2006.08.2941>
44. Gutman SI, Piper M, Grant MD et al (2013) Progression-free survival: what does it mean for psychological well-being or quality of life? Agency for Healthcare Research and Quality, Rockville. <https://www.ncbi.nlm.nih.gov/books/NBK137759>. Accessed 10 Dec 2017
45. Law M, Saindane AM, Ge Y et al (2004) Microvascular abnormality in relapsing-remitting multiple sclerosis: perfusion MR imaging findings in normal-appearing white matter. *Radiology* 231:645–652
46. Di Stefano AL, Bergsland N, Berzero G et al (2014) Facing contrast-enhancing gliomas: perfusion MRI in grade III and grade IV gliomas according to tumor area. *Biomed Res Int* 2014:154350. <https://doi.org/10.1155/2014/154350>
47. Scatliff JH, Radcliffe WB, Pittman HH, Park CH (1969) Vascular structure of glioblastomas. *Am J Roentgenol Radium Ther Nucl Med* 105:795–805
48. Scatliff JH, Guinto FC, Radcliffe WB (1971) Vascular patterns in cerebral neoplasms and their differential diagnosis. *Semin Roentgenol* 6:59–69
49. Jiddane M, Nicoli F, Diaz P et al (1986) Intracranial malignant lymphoma. Report of 30 cases and review of the literature. *J Neurosurg* 65:592–599
50. Hakyemez B, Erdogan C, Gokalp G et al (2010) Solitary metastases and high-grade gliomas: radiological differentiation by morphometric analysis and perfusion-weighted MRI. *Clin Radiol* 65:15–20
51. Xing Z, You RX, Li J et al (2014) Differentiation of primary central nervous system lymphomas from high-grade gliomas by rCBV and percentage of signal intensity recovery derived from dynamic susceptibility-weighted contrast-enhanced perfusion MR imaging. *Clin Neuroradiol* 24:329–336. <https://doi.org/10.1007/s00062-013-0255-5>
52. Ferreri AJM, Blay J-Y, Reni M et al (2003) Prognostic scoring system for primary CNS lymphomas: the International Extranodal Lymphoma Study Group experience. *J Clin Oncol Off J Am Soc Clin Oncol* 21:266–272. <https://doi.org/10.1200/JCO.2003.09.139>
53. Roth P, Martus P, Kiewe P et al (2012) Outcome of elderly patients with primary CNS lymphoma in the G-PCNSL-SG-1 trial. *Neurology* 79:890–896. <https://doi.org/10.1212/WNL.0b013e318266fcb2>
54. Valles FE, Perez-Valles CL, Regalado S et al (2013) Combined diffusion and perfusion MR imaging as biomarkers of prognosis in immunocompetent patients with primary central nervous

- system lymphoma. *AJNR Am J Neuroradiol* 34:35–40. <https://doi.org/10.3174/ajnr.A3165>
55. Koeller KK, Smirniotopoulos JG, Jones RV (1997) Primary central nervous system lymphoma: radiologic-pathologic correlation. *Radiographics* 17:1497–1526
  56. Roser F, Saini M, Meliss R et al (2004) Apoptosis, vascularity, and proliferation in primary central nervous system lymphomas (PCNSL): a histopathological study. *Surg Neurol* 62:393–399
  57. Sugita Y, Takase Y, Mori D et al (2007) Endoglin (CD 105) is expressed on endothelial cells in the primary central nervous system lymphomas and correlates with survival. *J Neurooncol* 82:249–256
  58. Takeuchi H, Matsuda K, Kitai R et al (2007) Angiogenesis in primary central nervous system lymphoma (PCNSL). *J Neurooncol* 84:141–145
  59. D’Haene N, Catteau X, Maris C et al (2008) Endothelial hyperplasia and endothelial galectin-3 expression are prognostic factors in primary central nervous system lymphomas. *Br J Haematol* 140:402–410
  60. Heiland S, Benner T, Debus J et al (1999) Simultaneous assessment of cerebral hemodynamics and contrast agent uptake in lesions with disrupted blood-brain-barrier. *Magn Reson Imaging* 17:21–27
  61. Heiland S, Hartmann M, Sartor K (2000) Is perfusion MRI feasible in lesions with disrupted blood-brain barrier? Pitfalls and possible solutions. *Rofo* 172:812–816
  62. Rorden C, Brett M (2000) Stereotaxic display of brain lesions. *Behav Neurol* 12:191–200

## Affiliations

**Stella Blasel**<sup>1</sup>  · **Rieke Vorwerk**<sup>1</sup> · **Makoto Kiyose**<sup>1,3</sup> · **Michel Mittelbronn**<sup>5,8,9,10,11</sup> · **Uta Brunnberg**<sup>12</sup> · **Hanns Ackermann**<sup>13</sup> · **Martin Voss**<sup>4</sup> · **Patrick N. Harter**<sup>5,6,7</sup> · **Elke Hattingen**<sup>1,2</sup>

<sup>1</sup> Institute of Neuroradiology, Goethe-University Hospital Frankfurt, Schleusenweg 2-16, 60528 Frankfurt, Germany

<sup>2</sup> Neuroradiology, Radiology, University Clinics Bonn, Sigmund-Freud Strasse 25, 53127 Bonn, Germany

<sup>3</sup> Epilepsy Center Frankfurt Rhine-Main, Institute of Neurology, Goethe-University Hospital Frankfurt, Schleusenweg 2-16, 60528 Frankfurt, Germany

<sup>4</sup> Dr. Senckenberg Institute of Neurooncology, Goethe-University Hospital Frankfurt, Schleusenweg 2-16, 60528 Frankfurt, Germany

<sup>5</sup> Edinger Institute, Institute of Neurology, Goethe-University Frankfurt, Heinrich Hoffmann Strasse 7, 60528 Frankfurt, Germany

<sup>6</sup> German Cancer Consortium DKTK Partner Site, Frankfurt/Mainz, Germany

<sup>7</sup> German Cancer Research Center DKFZ, Heidelberg, Germany

<sup>8</sup> Luxembourg Centre of Neuropathology (LCNP), 3555 Dudelange, Luxembourg

<sup>9</sup> Department of Pathology, Laboratoire National de Santé (LNS), 3555 Dudelange, Luxembourg

<sup>10</sup> Luxembourg Centre for Systems Biomedicine (LCSB), University of Luxembourg, 4361 Esch-sur-Alzette, Luxembourg

<sup>11</sup> NORLUX Neuro-Oncology Laboratory, Department of Oncology, Luxembourg Institute of Health (L.I.H.), 1526 Luxembourg, Luxembourg

<sup>12</sup> Department of Hematology and Oncology, Goethe-University Hospital Frankfurt, Theodor-Stern-Kai 7, 60590 Frankfurt, Germany

<sup>13</sup> Institute of Biostatistics and Mathematical Modelling, Goethe-University Hospital Frankfurt, Theodor-Stern-Kai 7, 60590 Frankfurt, Germany